H2020 Grant Agreement N° 690835

Deliverable D3.3 – WP3 – Due date: 30 June 2017

Title: Mu2e laser system

Type: Report

Dissemination level: Public

WP number: WP3

Lead Beneficiary: INFN

Description:

The report on the design of the Mu2e calorimeter laser system has been released as a Mu2e document on October 13th 2017: Mu2e-doc-13508, “Requirements and Design of the Mu2e Calorimeter Laser System”.

The report is attached to this document.

Requirements and design of the Mu2e calorimeter Laser system

C.Ferrari

INO and INFN Pisa, Pisa, Italy

M.Cordelli, S.Miscetti, A. Saputi

Laboratori Nazionali di Frascati dell'INFN, Frascati, Italy

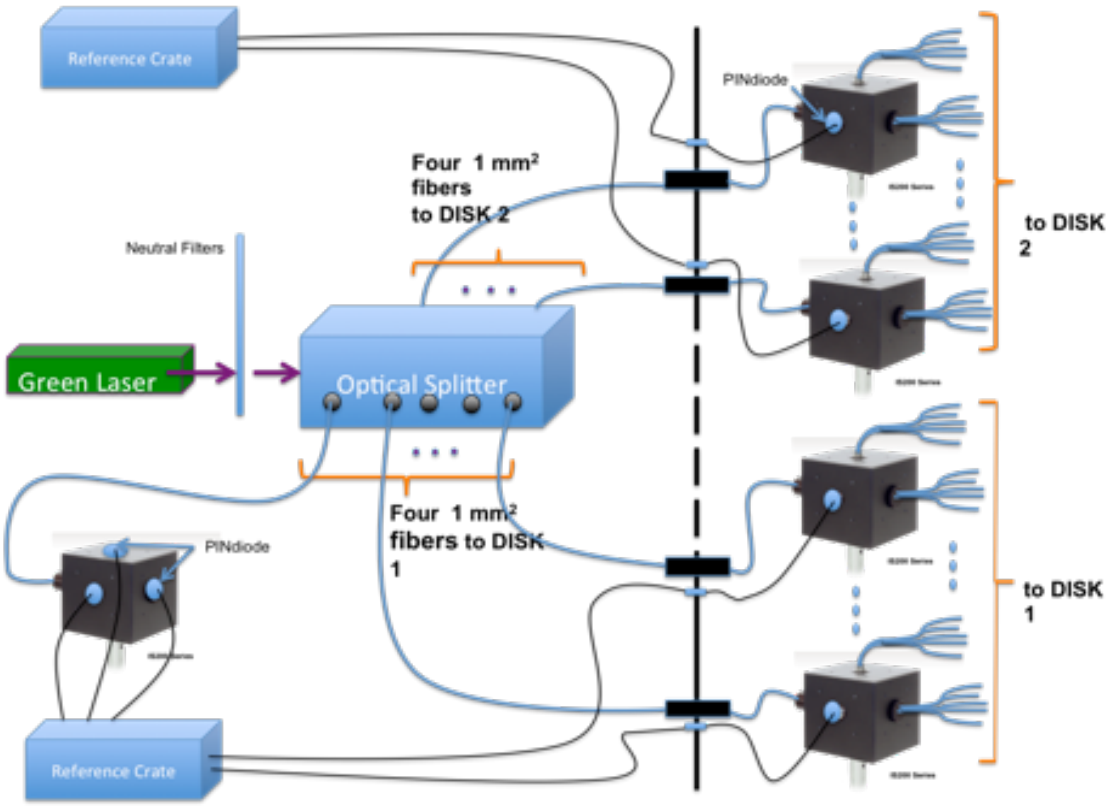

1 Requirements for the Mu2e EMC Laser Monitoring System

To keep the timing and energy resolution requirements for the calorimeter system [1], a redundant set of calibration tools are being designed. The crystal by crystal equalization is obtained by means of a calibration system formerly devised for the BaBar calorimeter [2], where a 6.13 MeV photon line is obtained from a short-lived ^{16}O transition. The decay chain come from the Fluorinert^{TM} coolant liquid that is activated by fast neutrons. The activated liquid circulates in aluminum tubes positioned in the front calorimeter plate to uniformly illuminate each crystal face. In-situ, we will rely also on cosmic rays [3] and decay in orbit (DIO) events to calibrate, with offline reconstruction, the timing and energy scales. However, conditions of running will be continuously changing due to irradiation of sensors. Our irradiation tests [4] indicate that both dose and neutron irradiation will contribute to deteriorate the calorimeter functionality providing: (i) a combined reduction of light yield and increase of radiation induce noise (RIN) on the crystals and (ii) an increase of leakage currents of the SiPMs. These running conditions will require a cool down of the sensors and a fast and continuous monitoring of the detector gains, of the timing offsets and of the energy and timing resolutions. *These tasks will be carried out by the Laser Monitoring System.* In the following the basic requirements for this system are summarized:

1. **Energy:** While a check of the absolute energy scale will be provided by the weekly source calibrations and by cosmic rays running, a control of faster gain changes (due to irradiation, increase of leakage current or temperature variation) is needed to keep the detector equalization constant. Since we expect slow variation trends, the relative gain change, at 0.5-1 % accuracy, can be tracked each few (tens of) minutes. A measurement of the light yield (via the ratio between left and right photosensors) and of the corresponding energy resolution will be also continuously performed.

2. **Timing:** Similarly the determination of channel by channel timing offsets, T_0, and the timing pulse height dependence (slewing) has to be carried out to compensate for small differences on cable lengths, transit times of SiPMs' response or electronics delays and jitters. In particular the synchronization of the clocks distributed to the calorimeter waveform digitizer will be done to keep timing calibration below few tens of ps. On the other side, a final alignment of the timing scale between calorimeter and tracker will be provided "in situ" only by means of reconstructing DIO electrons. A continuous monitoring of the timing resolution will be performed online with the laser system by means of the time difference between left and right photosensors.

In order to fulfill these requirements, the laser system has to satisfy these technical specifications:

1) It has to have enough power to get light to all 1374 crystals by means of an optical distribution system. We have designed the distribution system to get a laser signal at the photosensor end with a pulse height equivalent to a 100 MeV electron i.e. to a number of around 3000 photoelectrons (Npe)/photosensor.

2) It has to be able to track (with 1% precision) the variation of the light at the source and at the last distribution step by means of a monitoring system based on photodiodes.

3) The laser has to emit on blue or green wavelengths to be in a region far away from the CsI emission peak (310 nm). In this region, the transmittance changes due to irradiation are expected to be small. Comparing with the source running, this allows to isolate the response variation due to the change of photosensors'gain from the one related to crystal light yield reduction.

4) The laser has to be pulsed with a settable frequency below 100 Hz by means of an external trigger. During running the laser will be fired at a rate of 0.1 – 0.2 Hz and will be synchronized with the machine Clock in order to be acquired in the "beam-off" region.

5) The laser output has to be adjustable in amplitude to allow a measurement of the response linearity for the photosensors and for the FEE chain.

6) The monitoring system at the source will be based on photodiodes in a thermally controlled box.

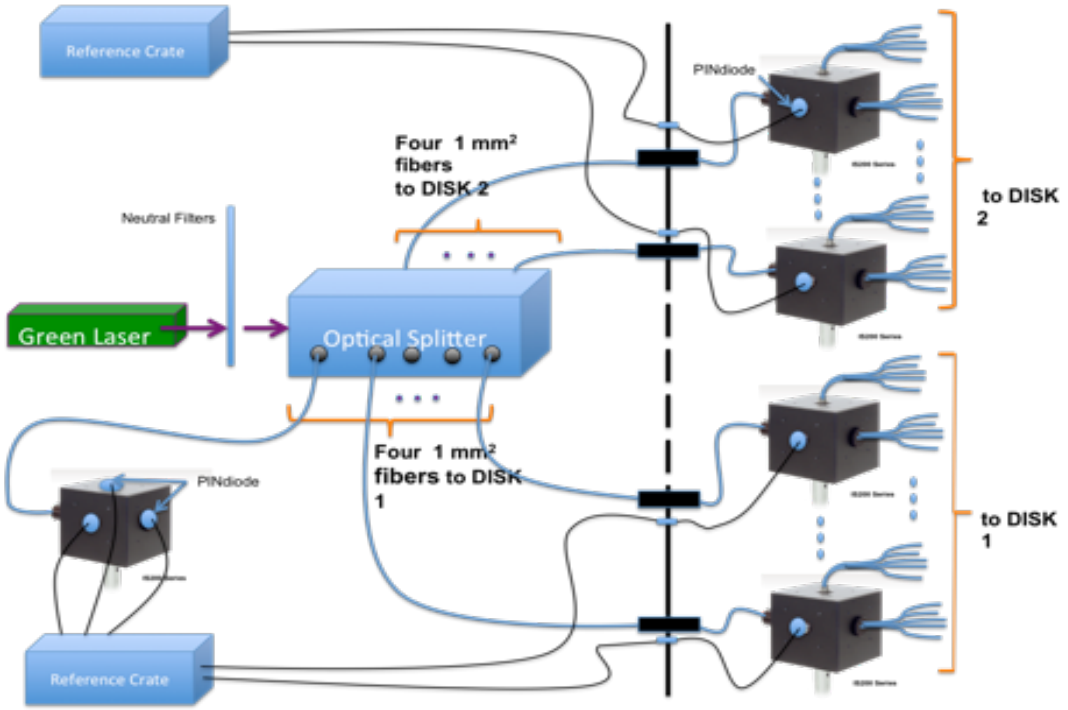

Figure 1: Laser System Schematic.

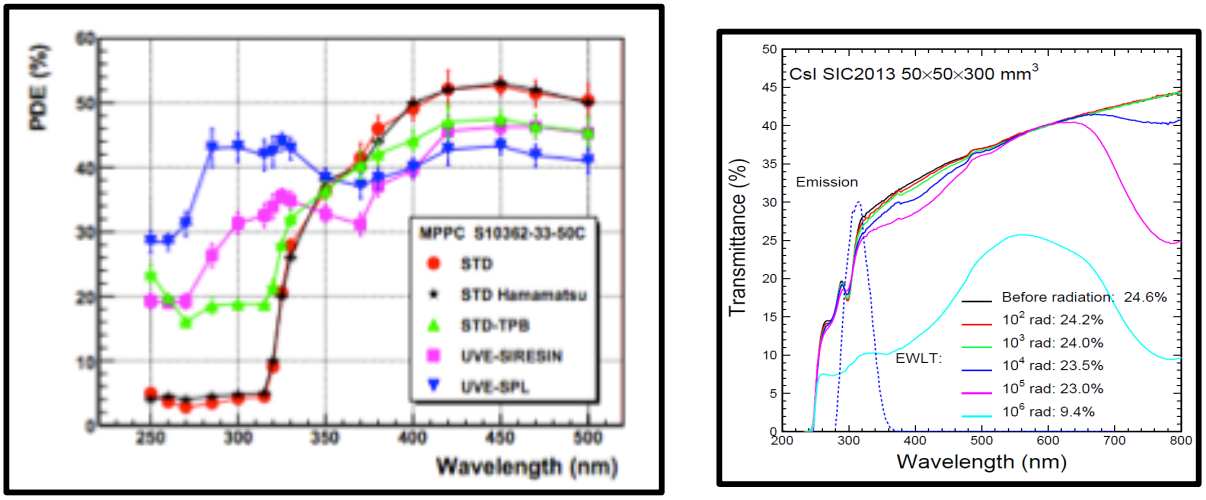

Figure 2: (left) PDE of SiPM, (right) CsI radiation hardness.

2 Design of the Mu2e EMC Laser Monitoring system

In order to continuously monitor variations of the response, timing and resolutions of each calorimeter SiPM, the Mu2e Laser System has been designed with a light distribution similar to the one used for the CMS calorimeter [5], see Fig. 1. The usage of SiPMs requires a laser emitting at a wavelength where the sensors have a high photon detection efficiency (PDE). Although the peak sensitivity of our SiPMs has been extended in the UV region, they keep an acceptable high PDE also in the green region

(Fig. 2.left). This is an advantage for our system since the deterioration of CsI crystal transmittance due to the irradiation (Fig. 2.right) is concentrated at the lowest wavelengths and it does not interfere with a calibration system tuned above 500 nm. The laser light is transmitted by a distribution system ending with 24 bundles of optical fibers, each fiber bringing light on the readout side of one specific calorimeter crystal. The fiber-end is encapsulated in a long custom made ferrule-connector that is then inserted in a guide inside the SiPM holder. The ferrule is kept in place, in a reproducible way, by a connector. The light is then transmitted to the crystal back face and then reflected and diffused (by the crystal itself and its Tyvek wrapping) to illuminate the active area of the sensor. Monitoring of the variation of the laser light will be performed in two places: (i) at the output source and (ii) at the end of the distribution system. This will be done relying on silicon photodiodes. In the following sections the single components of the Mu2e Laser system are described. Few technical choices between similar components are still pending and will be solved during the procurement phase in 2018, however these final choices will not modify the overall design of the system. In subsec. 2.1, we describe the light distribution system, from the Mu2e Laser output to the fiber-ends in the SiPM holders. In subsec. 2.2, we describe the monitoring system of the laser output. In subsec. 2.3 we calculate the laser power needed to satisfy our requirements. In subsec. 2.4 we list the kinds of laser that can satisfy the power and all other requirements. Finally, in subsec. 2.5, safety considerations are discussed.

2.1 The Mu2e Laser Light distribution system

A schematic of the light distribution system is shown in Fig. 1. A high-precision, high-power, pulsed laser sends light through a 12-positions filter wheel to an optical splitting system, to subdivide the beam into 10 equal parts: 8 beams will be sent to the two disks (4 each disk), while other 2 beams will be reserved for monitor of the source laser output.

2.1.1 Primary light distribution system (at the source)

There are three alternative methods for splitting the laser beam:

1) **Standard optics.** The most flexible solution with standard optics has been realized using the following components: (i) non-polarizing cube beam splitters, Thorlabs mod. BS010; (ii) mirrors; iii) collimators, Thorlabs mod. CFC-8X-A. The system is composed of 9 non-polarizing cube beam splitters, 10 mirrors and 8 collimators. This solution requires an optical table of dimension 100×150 cm^2. A drawing of this option is shown in Fig. 3.
2) **Fiber Port Clusters from Schäfter+Kirchhoff** (Fig. 4.left). The technical description is found at (https://www.sukhamburg.com/download/research_e.pdf).

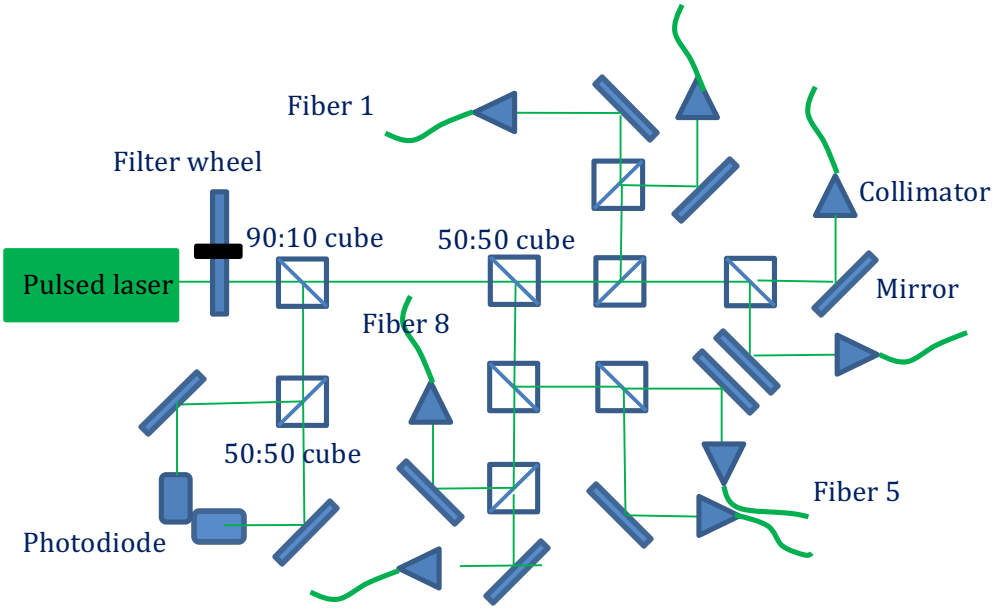

Figure 3: Schematic drawing of the Optical Distribution system.

The optical power carried by a polarization-maintaining single-mode fiber is split into multiple polarization-maintaining single-mode fibers with high efficiency. Compared to option (1), this approach presents a higher cost, but various advantages: i) closed system protected from dust and accidental hits, ii) greater stability; iii) a much smaller footprint with consequent savings on the cost of the optical table and the interlock system.

3) **Planar light circuit.** This is a planar waveguide technology for 1x16 splitting (Fig 4. right). An example is provided by a Leoni-fiber optics splitting system as (http://www.leoni-fiber-optics.com/uploads/tx_downloadleoni/en_fibersplit.pdf). This PLC option have some advantages of option (2) but an affordable cost.

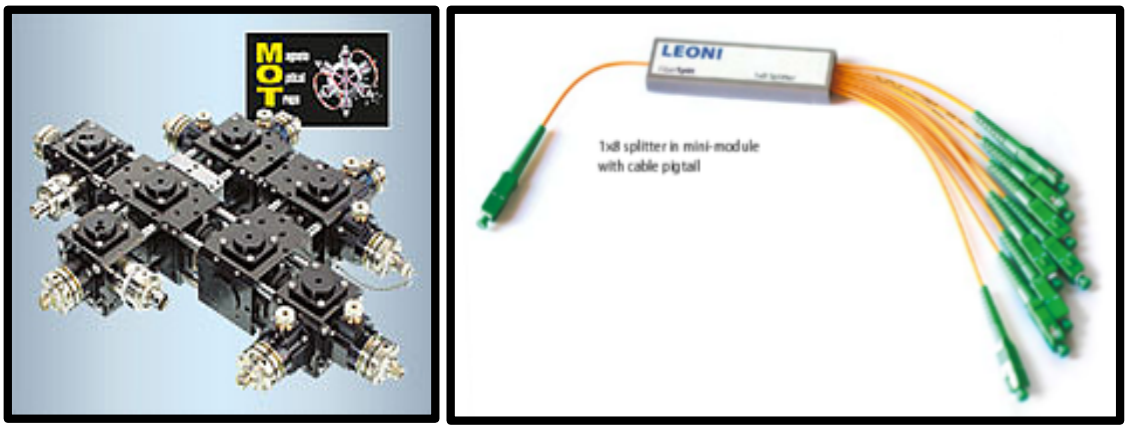

Figure 4. Fiber Port Clusters (left); Planar light circuit (right).

A single-mode beam is mandatory in options (2), to ensure a stable splitting ratio over time. Also option (3) will benefit of a single-mode laser, reducing the coupling fluctuation between different channels. As a matter of fact, the requirement in uniformity between the various beams is not very large, we have set this requirement to be of ± 10%, knowing that the uniformity of the secondary distribution system with integrating sphere and bundle of fibers will not be better than this. What we are looking for it is instead stability along running time. Whatever is going to be the light arriving to the crystals, we then aim for a time-stability of ± 1 % on its distribution. Following this consideration, option (2) is the most performing choice, since it has been developed for very harsh operating conditions (such as space flights). However, this option has a related high cost. On the contrary, the simpler and cheaper solution is the PLC split fiber system. We have a prototype of this splitter in our laboratory to measure its uniformity and stability. After carrying out this measurement, we will take a decision to down-select these options.

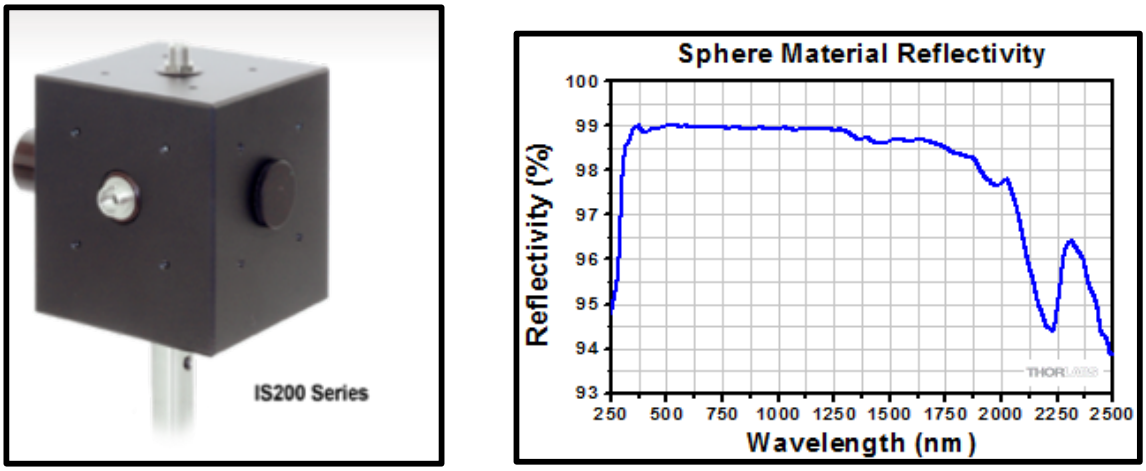

Figure 5: (Left) Thorlab diffusing sphere. (Right) Sphere reflectivity as a wavelength function.

2.1.2 Secondary light distribution (from primary to fiber bundles)

By means of eight 400 μm diameter, 60 m long quartz fibers *(launching fibers)* the light is then brought from the laser head, located in the T-DAQ room, to the Detector Solenoid bulkhead (IFB) and then through vacuum feed-throughs to the back face of the calorimeter disks. Two kinds of feed-throughs are being selected with similar performance. They will be tested in our small size dewar for Module-0:

1) (https://www.sukhamburg.com/products/Vacuum_Feed-Throughs_V-html)
2) AVANTES-FC-VFT connectors.

The diameter of the fibers (400 μm) has been selected since it grants a good transmission performance and a lot of flexibility in operation. In particular, these fibers have better bending radius with respect to 1 mm diameter fibers. *The launching fibers* will be protected by their own external cladding and routed inside "corrugated-pipes". Shorter fibers (of ~10 m) will be routed inside the DS to reach the diffusing system on the disks.

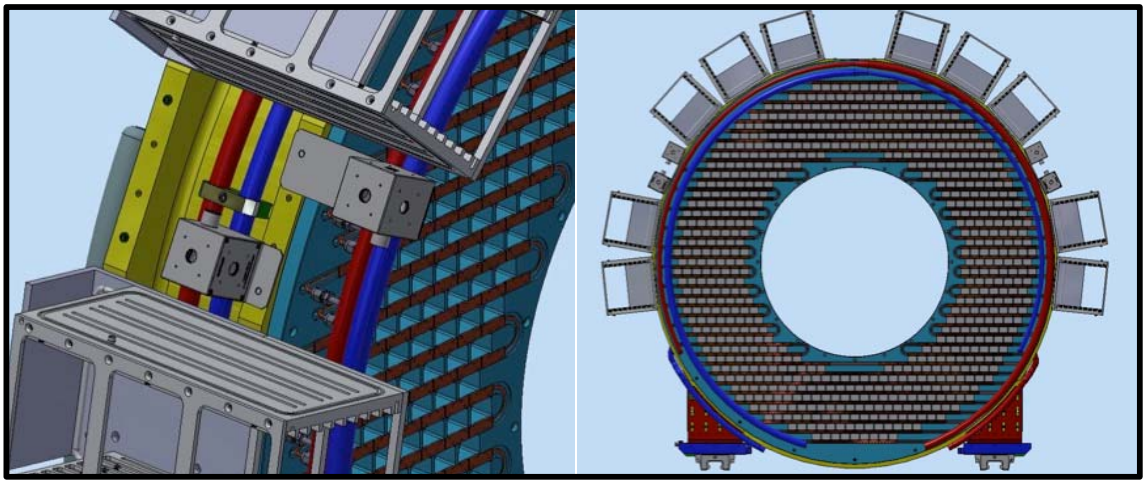

Figure 6: (Left) Positioning of spheres in the outer disk and (right) disk transversal view.

On each disk, there are four integrating spheres (see Fig. 5) with one input port for the launching fiber on the top, three outputs and one detector port close to the crates. The selected sphere, **Thorlabs, mod. IS200-4, Ø2" Integrating Sphere** (No Sensor, 4 Ports) is resistant to heat, humidity and high levels of radiation. It has also a very high reflectivity at 500 nm. Running from each one of 3 output ports, there is a bundle of 70, 200-µm diameter fused silica fibers, for a total of 840 fibers/disk. Of the 840 fibers/disk, 674 are used for SiPMs calibration, while the remaining 166 (25%) are used as replacements in case fibers get broken during handling. The position of the spheres on the disk is shown in Fig. 6. In the left picture, there is a zoom of the two spheres.

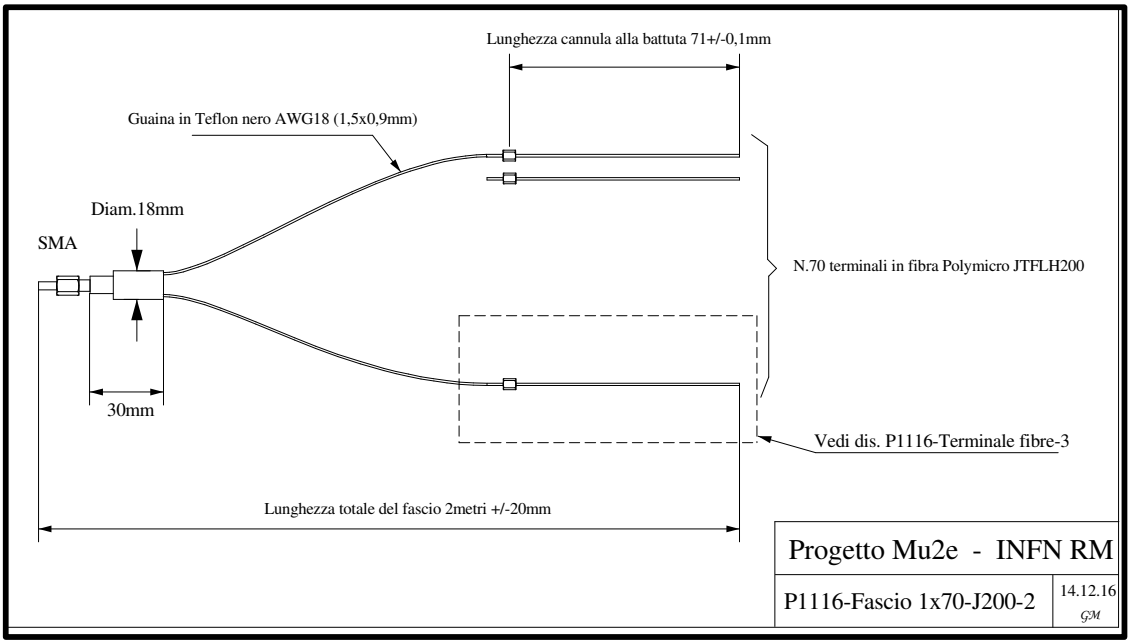

Figure 7: Design of the fiber bundle.

The *launching fiber* will arrive on the front calorimeter face routed from the IFB to the top section of the calorimeter disk, together with LV and HV services. We have two spheres/calorimeter side, for a total of 4 spheres/disk. We are still optimizing with the CAD the final position of these sphere in order to eliminate any interference with the tracker alignment system.

2.1.3 Design of the bundle of fibers and fiber ferrule

There is a stringent requirement on the fibers. They should have high transmission at 500 nm and they must be radiation hard up to O(100 krad). The best choice is fused silica.
The 70 fibers in the bundle (Fig. 7) will have a length of around 200 cm, and will be grouped together in an SMA-905 connector, for easy plugging on one port of the integrating spheres, and with a special ferrule connector on the other side. The best choice is a **JTFLH2002305000 fiber**, with a silica core diameter of 200 um, a polymeric cladding of 230 um diameter and an external Teflon protection of 500 um diameter. The fiber will be glued inside a custom-designed ferrule in stainless-steal AISI 304. All fiber ends will be polished. The fibers have a numerical aperture, NA = 0.37. The fiber insertion in the SMA-connector and in the custom ferrule will be protected with a Teflon coverage. All materials used are low outgassing (Teflon, stainless steal). The glue resin, ASTM E595, is respecting the quality tests ASTM E595 from NASA. A prototype is under procurement to make a direct test of the outgassing level. Nevertheless the procurement of all bundles will be done with an open tender requiring very tight technical specifications. In Fig. 8, a conceptual drawing of the basic insertion of the custom-designed ferrule in the SiPM holder is shown.

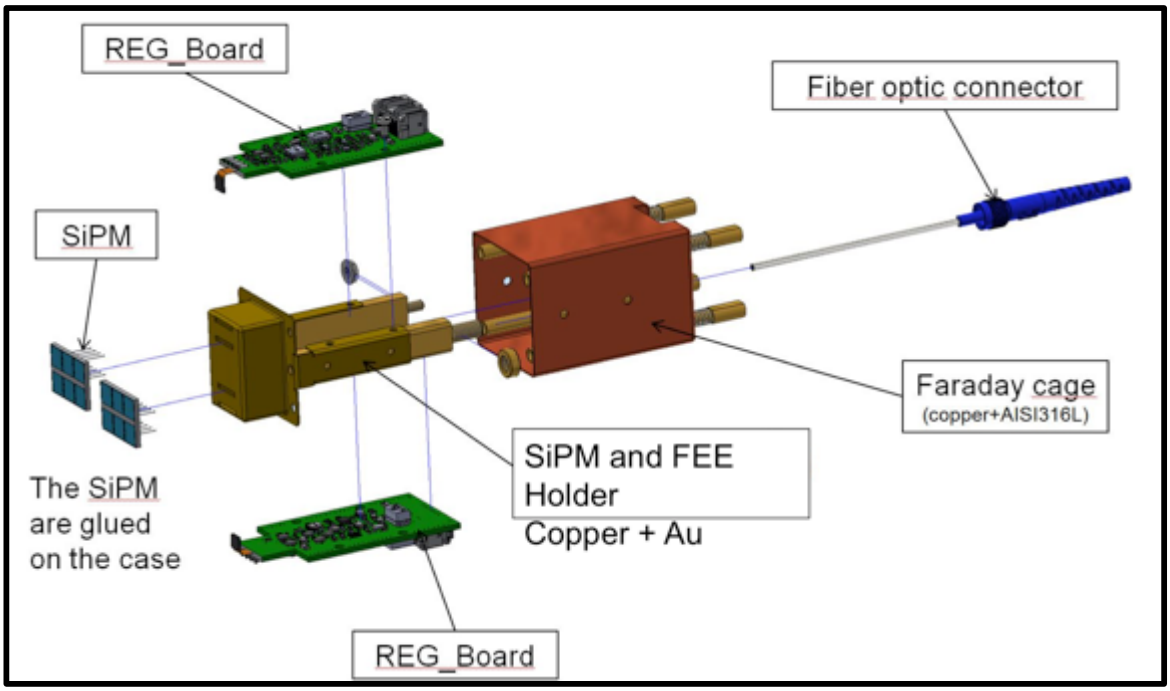

Figure 8: Conceptual design of the custom ferrule and its insertion in the SiPM holder.

2.2 The Laser Light Monitoring System

The light output from the laser system is monitored with phodiodes that will measure:

i) the output of the laser light at the primary splitting system;

ii) the light at the secondary distribution spheres at the detector port of the diffusing spheres.

A total of 8 + 8 photodiodes are needed. The first eight will monitor the two spare beams in the primary distribution system (four per beam), the last eight will monitor the light arriving to each integrating sphere. These photodiode monitors are required to track pulse amplitude variations larger than 1%. The photodiode have unitary gain so that we have not stability problem. Four different Hamamatsu photodiodes are being tested at the moment of writing as listed here:

1. S1226-5BK;
2. S2386-44K;
3. S1227-1010BR;
4. S1127-33BR1.

The signal at the laser input will be so large that we do not need any amplification. However, we are still evaluating if needing or not an amplification system at the end of the secondary distribution system. An amplifier for these photocells have been already produced for the g-2 experiment by the SEA department at LNF. We will test the response of the photocells with and without amplification. If we will find out that this is needed, this will correspond to arrange locally four additional LV cables from a modified calorimeter mezzanine board (MB) in the calorimeter crates. Readout will be done with a MB+digitizer calorimeter board/disk. The laser and the monitor boxes at the primary distribution system will be temperature controlled to reduce the variation of the laser output to a few percent and to minimize the photodiode temperature correction. Variation of the leakage current is instead expected at location of the secondary light distribution as related to the neutron fluence reached in the area. We will evaluate the most radiation hard sensors (from the list above) with a direct neutron irradiation test. If the leakage current will become too large after one year of running, we can replace the sensors during each shutdown to reduce this problem.

In order to monitor the calorimeter response linearity and calibrate the gain with the standard method of photoelectron statistics, a neutral filter wheel, with gradually changing absorption values, is inserted between the primary beam and the light distribution system **(Thorlbas, mod. FW212CNEB, Twelve-Position Motorized Filter Wheel for Ø1/2" (Ø12.7 mm) Optics with Preloaded ND Filters).**

2.3 Evaluation of Laser pulse characteristics (width, power, stability)

There is not a stringent requirement on the laser pulse width, since both the SiPM and photocell readout electronics have a bandwidth of about 100 MHz, thus setting an upper

limit on the width of few ns. Similarly, we do not have a strong requirements on the pulse frequency since, as shown in the prototype tests (sec. 3), running at O(1 Hz) provides better than per-mil statistical precision in one hour of data-taking. On the other hand, using the laser at low rate will reduce the consumption of the laser head and the need for replacement. It is instead mandatory to synchronize the laser pulse with an external trigger in order to allow the light reaching the detector at the correct time relative to the proton beam pulse. We intend to acquire laser data in the beam OFF period and for special running when the calorimeter is acquiring physics data. This will be further discussed in sec. 4.

Due to our choice of using diffusing spheres for the light distribution, the laser pulse energy is strongly attenuated at the end of the chain. The laser signal at the SiPM readout level is required to simulate a 100 MeV energy deposition. For un-doped CsI (30 pe/MeV) this corresponds to ~3,000 p.e. collected by each photosensor. The energy of a single photon at 500 nm is about 0.4 aJ, so that the laser pulse energy needed at the photodetector level should be 1.2 fJ. The transmission of the integrating sphere, using 200 nm optical fibers, is of 10^{-5}. The transmission of the other optical components is conservatively estimated as follows: 0.5 for the laser-fiber collimator, 0.7 for the 60 m launching fibers, 0.8 for the vacuum feed-throughs, 0.5 the loss inside the crystal, 0.18 for the average SiPM collection area and 0.2 for the average SiPM PDE on the green. The total transmission factor will then be: $5 \times 10^{-3} \times 10^{-5} = 5 \times 10^{-8}$, i.e. a reduction factor Rlight of 2×10^{7}. The laser pulse energy to be feed in each collimator in the primary distribution chain is 1.2 fJ x Rlight = 1.2 x 2 x 10 nJ = $10^{-8}/5$ = about 24 nJ. This roughly translates to a 0.25 μJ laser pulse energy (8 + 2 optical fibers). A safety factor of 10 is designed into the system to account for the eventual degradation of the signal transmission with time and to provide a larger power available when running outside the DS at room temperature. **This translates in a laser energy pulse requirement > 2.5 μJ.**

Figure 9: (left) STA-01SH2 laser, (right) Integrated Optics laser with cooling box.

Adjustment of laser power during running will be done in two ways: (1) by adjusting the control knob to select the wanted laser power output from the laser source and (ii) by a fine tuning provided by remotely selecting the wanted attenuation filter of the filter wheel.

2.4 The laser source

We have carried out a search on the market to evaluate different options for a laser source with the following characteristics:

- A pulsed laser emitting green light (from 500 to 550 nm) with pulse width < 5 ns;
- A programmable repetition rate (< 50 kHz), with a TTL external trigger;
- A pulse energy above > 2.5 μJ;
- O (3 %) pulse to pulse stability;
- Adjustable in power output;
- Single mode;
- Spatial mode TEM_{00};
- A time jitter below 3 ns.

We have found 3 laser sources (see pictures in Fig. 9) satisfying our requirements.
The first one (STA-01SH2) is at the edges of our acceptance choice since it does not provide a simple adjustment in power amplitude. We have reported it here, since we have used it on the prototyping phase. During 2018, we will make a final selection of the laser source with a tender phase. For the moment, we will assemble one vertical slice of the distribution system using the prototype source. All laser sources selected present a drift over running time, after 5' warm-up, that is below 5 %. The pulse to pulse stability in short period is excellent as required. During running, we assume to keep the laser source in an AC conditioned room. If this is not possible, we will provide a Peltier-controlled box, connected to an Al radiation, to keep the Laser head at a stable temperature.

Table of Typical Micro Laser Models

Models	STA-01SH-1	STA-01SH-2	STA-01SH-3	STA-01SH-4	STA-01SH-5
Wavelength, nm			532		
Average output power (max), mW	40	25	50	20	100
Pulse energy, μJ	4	5	50	0.2	100
Pulse width (FWHM), ns	0.5	< 0.7	0.5	0.5	0.5
Repetition rate (max), kHz	10	5	1	100	1
Beam Profile			$M^2 < 1.1$		
Pulse spectral structure			single longitudinal mode		
Polarization ratio			> 100:1		
Beam Waist diameter inside the laser head $1/e^2$, μm*			25-200		
Pulse spectrum FWHM, pm			< 5 (near transform limited)		
Pulse to pulse energy stability RMS			< 0.5		
Power stability over six hours**			< ± 1,5%		
External power supply voltage, V AC			100-240		

Figure 10: STANDA Laser parameters.

1) **Standa,**
   The prototype laser STA-01HS2 had a short pulse duration, a good stability along time and satisfied the requirement for power (See Fig.10).

2) **CryLas,** mod. FDSS532-Q2, Diode Pumped Passively Q-Switched Solid State Laser (http://www.crylas.de/productsheets/FDSS%20532-Q_Rev2.3_1.2015.pdf): 6 µJ @ 10 kHz, Pulse-To-Pulse RMS < 2% @10kHz, Pulse duration 1.3 ns. Summary of characteristics are in Fig.11.

3) **IntegratedOptics,** mod. 515L-21C, 514.5 NM NANOSECOND SLM LASER (https://integratedoptics.com/nanosecond-lasers/5145-nm-nanosecond-slm-laser): 3 µJ @ 16 kHz, Pulse-To-Pulse < 2%, Pulse duration 3 ns. This Laser Head is also TEC controlled for laser diode temperature. Connection with an Al radiator is already available as accessory.

Optical Data		**FDSS532-Q1**	**FDSS532-Q2**	**FDSS532-Q3**	**FDSS532-Q4_1k**
	Wavelength	532 nm			
	Pulse Energy	> 2 µJ @ 15 kHz	> 6 µJ @ 10 kHz	> 20 µJ @ 1 kHz	> 42 µJ @ 1 kHz
	Peak Power	> 1.5 kW @15kHz	> 4.5 kW @10kHz	> 15 kW @ 1kHz	> 30 kW @ 1 kHz
	Pulse Repetition Rate	≤ 20 kHz	≤ 10 kHz	≤ 2.5 kHz	≤ 1 kHz
	Pulse Width, FWHM	≤ 1.3 ns			
	Polarization Ratio	> 100:1 vertical			
	Pulse Energy Drift [1)]	< ± 5 %	< ± 5 %	< ± 5 %	< ± 5 %
	Pulse-To-Pulse RMS [2)]	< 3% @15kHz	< 2% @10kHz	< 2% @1kHz	< 2% @1kHz
	Laser Classification	3B / IIIb	3B / IIIb	3B / IIIb	3B / IIIb
Optical Output	Spatial Mode	TEM_{00}			
	Beam Divergence, 2Θ	< 3.5 mrad	< 3.5 mrad	< 3.5 mrad	< 4.5 mrad
	Beam Diameter	250 ± 50 µm	260 ± 50 µm	300 ± 80 µm	400 ± 100 µm
Electrical Data	Power Consumption	15 W (max.40 W)	17 W (max.40 W)	20 W (max.70 W)	40 W (70 W)
	Operating Voltage	12 V DC			
	Line Voltage	90 - 265 V AC			
	Marking	CE			
Interfaces	RS 232, USB				
	External Trigger (TTL, rising edge) single shot (pulse on demand) – max. repetition rate				
	Interface for TTL-control and power monitor				
Miscellaneous	Warm-up Time	< 5 min			
	Operating Temperature	18 - 38 °C			

Figure 11: Crylas parameters

2.5 Safety considerations for the laser monitoring system

All the selected laser sources are in safety class 3-B, when considering the required energy per pulse and the maximum available repetition rate (tens of kilohertz). This type of laser source requires an interlock system, which includes all the air beam part, so Laser Head + Filter Wheel + Collimator System will be enclosed.

The rest of the optical system is either fiber-optics or otherwise enclosed (integrating spheres) and does not present any significant problems by providing a separate channel system for optical fibers, so preventing the risk of unforeseen breakage and possible light leakage.

The final bundle fiber optic pulse energy is extremely weak (pJ) and is not a threat to operators.

The only point at risk, to be handled with appropriate signage, is represented by the output of the 400 μm optical launching fibers that connect to the input of the integrating spheres (and that are also connected to the vacuum feed-throughs): here the pulse energy is more relevant and the disconnection of the optical fibers represents a risk.

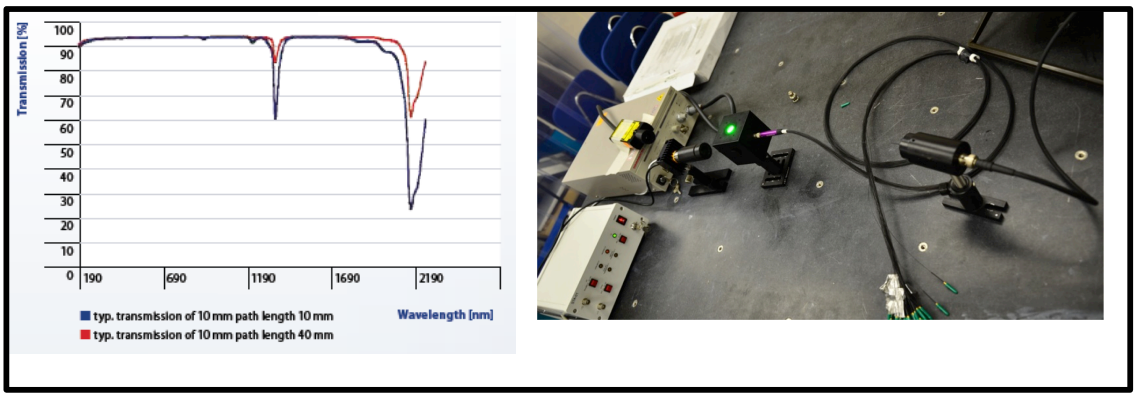

Figure 12: Transmission as a function of wavelength for fused silica fibers (left) and a picture of the light distribution system prototype (right).

3 Prototypes of the Mu2e Laser Monitoring system

3.1 Laser monitor prototype for the LYSO crystals

The setup used for the transmission test and for the calibration of the LYSO calorimeter prototype [6] is shown in Fig. 12.right. The light source was an STA-01HS2 solid-state pulsed laser emitting at 532 nm with a pulse energy of 20 μJ, a pulse width < 1 ns, good pulse-to-pulse stability (3%), and synchronization to an external trigger for frequencies up to 100 kHz. The prototype distribution system used a 2" integrating sphere, the ThorLab-IS200, with one input port and 3 output ports. Each of the output ports has a 0.5" diameter. Pictures of the sphere and of its reflectivity diagrams are shown in Fig. 5. An Hamamatsu photodiode S1722-02 is mounted on one Sphere port to monitor the laser pulse variation, while a bundle of fifty 2 m long, Leoni fused silica fibers of 200 (400) μm diameter core (core plus cladding) is inserted with an SMA connector to another port.

The number of photoelectrons, Npe, observed at the end of the transmission line has been determined by a direct measurement of the APD charge seen in the calorimeter. The input laser source was first reduced by a factor T_{filter} = 200 by means of a neutral density filter, in order to avoid signal saturation. The average APD charge, with the APD gain set to 50, was around 120 pC, with a channel-by-channel spread of ± 10%. This corresponds to Npe = 33,600, a factor of 3 more than required in the BaF_2 case. However, this determination does not take into account the reduction factor of 14 that results from the initial optical splitting system. The measured Npe is consistent with the pulse energy and distribution losses. One photon at 520 nm corresponds to $4x10^{-19}$ J, so that in a single laser pulse ~10^{12} photons are produced. Using the measured T_{fiber} and T_{filter}, the light transmitted at the end of the chain is estimated to be N_{photon}= 10^{12} x ($7x10^{-5}$) x 0.005 = 3.5 x 10^5. Correcting this estimate for the APD quantum efficiency of 70% and for the APD/crystal area ratio of 1/9, 27,000 detected photoelectrons are expected, in reasonable agreement with the measurement.

The prototype calibration system has been tested by measuring the transmission at one of the output ports, T_{port}, and by measuring the transmission at the end of the fiber bundle, T_{fiber}. The transmission in one port can be written as $T_{port}=(S_{port}/S_{sphere})\bullet M$, where S represents the surfaces and M=R/(1-R X (1-f)) is the sphere multiplication factor. R is the sphere reflectivity and f is the ratio between the ports and the sphere surfaces. At λ > 400 nm, R is 98%, f is ~5% and M is ~16, so that the transmission factor is ~0.012×16=0.192. The first measurement was performed by calculating the ratio between the light emitted by the laser and the light exiting the sphere port. A calibrated photocell of 13 mm diameter has been used, positioned at zero distance from the hole. The transmission measured is ~0.12, in reasonable agreement with our simplified model. Similarly, the transmission at the end of the fiber bundle has been measured, resulting in an average

factor of $T_{fiber}=7x10^{-5}$ that, as expected, is much better than the product of the simple geometrical ratio, 10^{-5}, and the fiber numerical aperture. The spread of transmission values for the best 43 fibers in the bundle has a $\sigma = 8\%$. The seven remaining fibers were accidentally cracked before the test, showing deviations worse than a factor of two.

Finally, in Fig. 13(left), the variation of the observed laser pulse as a function of the running time is shown. The average laser fluctuation observed in 12 hours of running has a σ ~5% and is mainly due to the variation of the APD response. This is shown by comparison with the reference pin-diode (green circles), which is much flatter than the calorimeter response. The residual fluctuation of the calorimeter to pin-diode ratio is 3.5%. This is much worse than the ratio between two calorimeter channels (red points) that is at a level of 0.4% and of the PIN-diode, which is 1.6%. To confirm this, the dependence of the calorimeter response on the temperature has been studied by measuring the temperature in the APD region with a PT-100 probe (Fig. 13.right). The APD gain dependence on temperature is consistent with the observed residual calorimeter/pin fluctuation as shown by the anti-correlation between the APD temperature and the calorimeter response in Fig. 13.right. The gain variation of the APD corresponds to ~ - 4 %/C°.

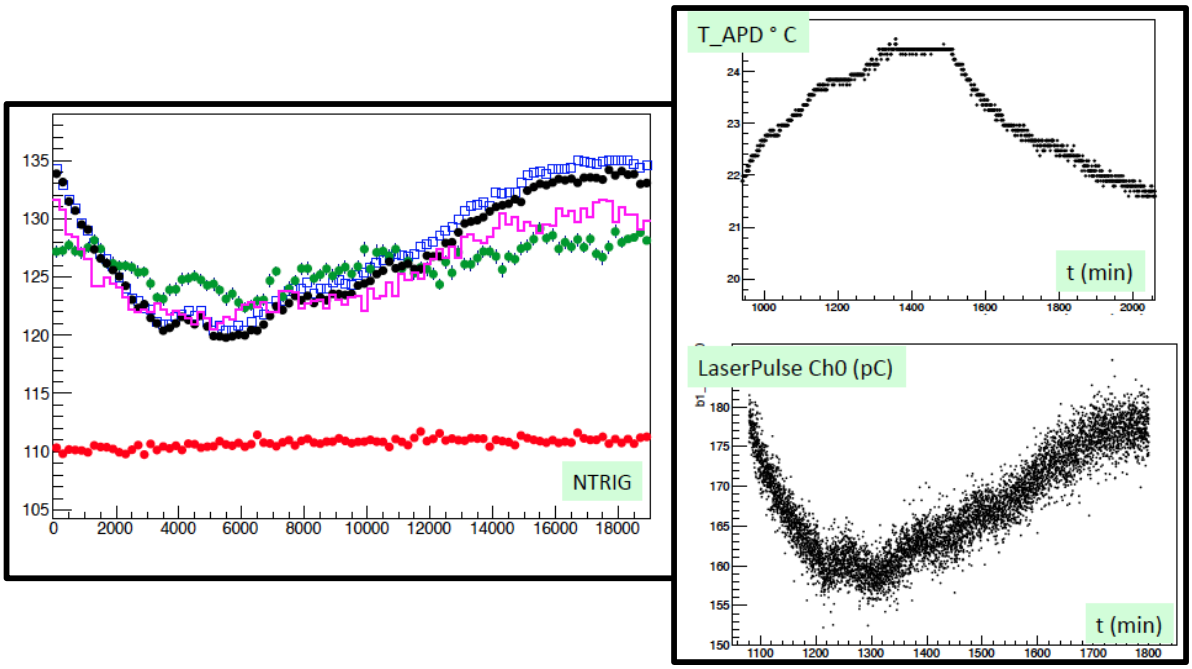

Figure 13. The left plot shows the distribution of the average laser pulse energy as seen by two calorimeter channels as a function of the trigger number (black and blue points), of the average pin diode response (green points) and of the ratio between the calorimeter channels (red points). The purple histogram shows the ratio between calorimeter channels and the PIN-diode, isolating the residual fluctuations of the APD gain. Also shown is the distribution of the temperature as a function of running time in minutes (top right), and the variation of the laser pulse for channel 1 during the same period (bottom right).

3.1 Laser monitor prototype for Module-0

After freezing the design of the calorimeter system [7], we have proceeded in the assembly of a large size calorimeter prototype (dubbed Module-0) with all final components. The sketch of this calorimeter is shown in Fig. 14. The calorimeter is composed of 51 pre-production un-doped CsI crystals and 102 Mu2e custom SiPMs with FEE pre-production chips. Module-0 was assembled in April 2017 and tested for a week with an electron beam in May 2017 [8]. We did not have a complete fiber bundle with

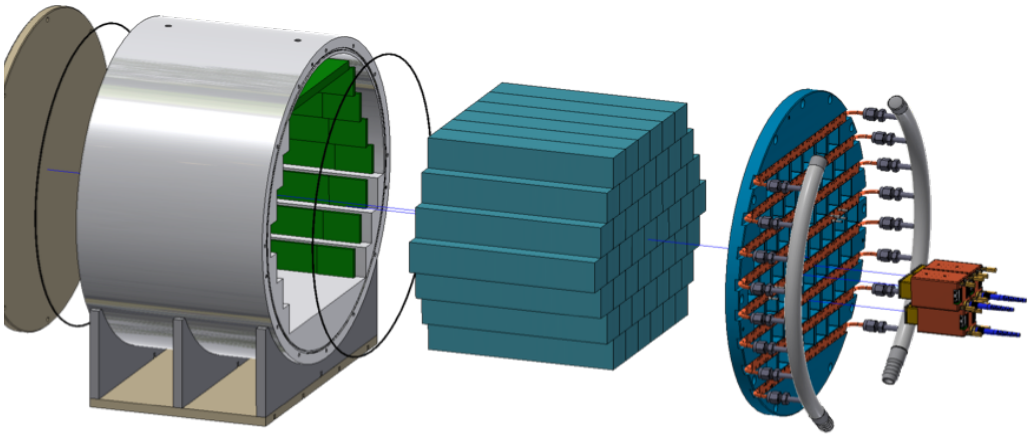

Figure 14: CAD of module-0.

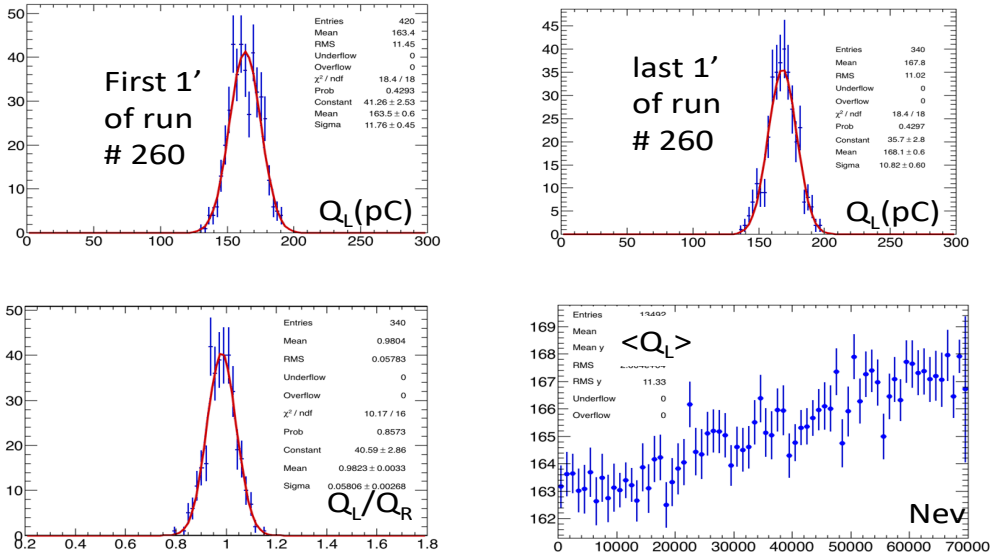

Figure 15: Laser resolution plots. Precision in the first (top-left), last (top-right) minute. (Bottom-left) L/R ratio between Left and Right SiPMs and (bottom-right) variation of response along running time.

custom-made ferrules completed at the test beam time, so that we could not exercise the lase system on all channels. However, we had prototyped one of these fibers and used it to test the system behavior by inserting the ferrule in the central crystal SiPM holder.

The first test was that of controlling the precision of the laser in monitoring the gain variation related to temperature. In Fig. 15.top, the distribution of the central crystal pulse height is shown for the first (left-plot) and last minute (right-plot) of a 30 minutes' run. The laser was fired at 7 Hz, so to acquire around 400-440 events/minute. The relative precision on the mean, reached in 1', was of 0.3-0.4%, thus allowing to clearly appreciate a variation of 1.5 % on the mean. Changes on the response was consistent with the temperature stability of the cooling system that presented a maximum variation ± 1 °C. The profile histogram of Fig. 15.bottom-right shows the trend of the response variation along the time.

The precision obtained is related to the number of photoelectrons reaching the sensor; this has been estimated by the width of the ratio (L/R) distribution between the Left and Right SiPMs reading out the central crystal. Indeed, the L/R ratio eliminates the contribution due to the laser fluctuation and is related to the number of photoelectrons seen by a single sensor (Npe) as follows: Sigma(L/R)/(L/R) = SQRT(2/Npe). Npe is then derived as Npe = 2 x $[(L/R)/(\text{Sigma}(L/R)]^2$, thus corresponding to around 600 pe, i.e. a signal equivalent to 20 MeV energy deposit in the CsI crystals. Intrinsic Laser precision with this light yield is of 4% per event.

This prototyping allowed us to estimate the laser firing frequency during experiment running. As a basic guideline, to reach precision of 1% we need to acquire around 16-20 events. Even running the laser at a frequency of 0.2 Hz, we need only 80-100 seconds to reach this precision.

4 Integration in the experiment and TDAQ considerations

The T-DAQ will generate a continuous Mu2e system clock [9] with frequency of 40 MHz at the run-control host Clock FanOut Module (CFO). The CFO receives also all needed markers from the accelerator division. The CFO outputs an encoded clock indicating the start of the Mu2e event window (see Fig. 16.Top). The spill of beam ON will consists of 25000 proton pulses. A Super-cycle will consist of 380 ms of 8 spills of beam ON and 1020 ms of beam OFF (see Fig. 16.bottom).

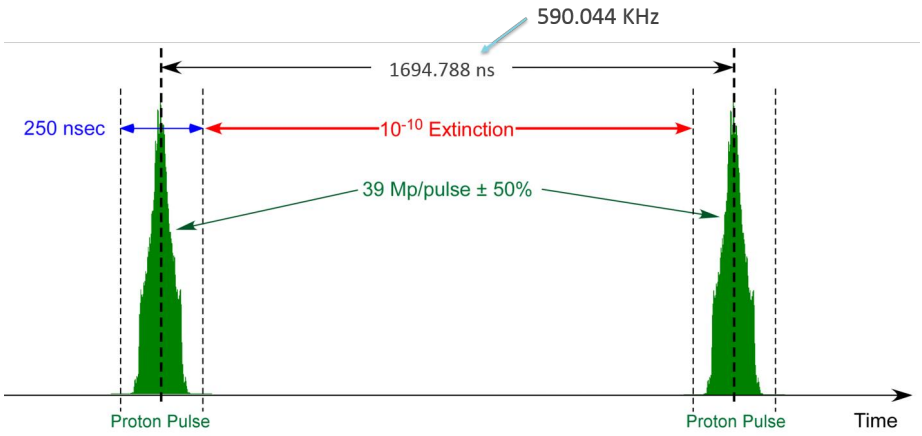

Figure 1. A spill consists of ~25,000 proton pulses (250ns wide) spaced by 1695ns.

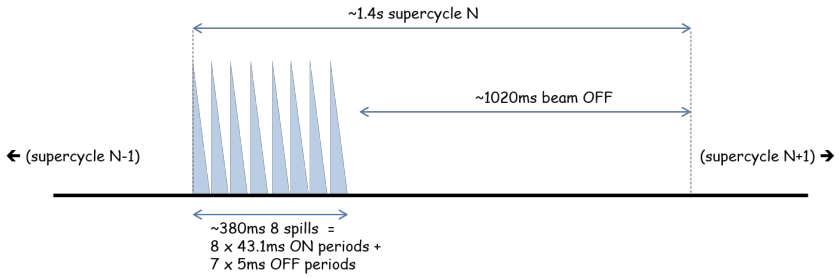

Figure 2. The anticipated supercycle timeline is ~1.4 s and consists of 8 spills each spaced by 5 ms. The phase of proton pulse arrival may change for each spill.

Figure 16: Timing of accelerator signals in Mu2e: (top) Microbunch structure, (bottom) Super-cycle structure.

We will receive from the TDAQ one copy of the encoded clock and a Control Optical Link. Our plan is to drive the laser system at very low frequency (0.1-0.2 Hz) and synchronize the arrival time of the calibration signals in a beam off period. Specific markers can be sent by the T-DAQ in the beam-off period and will be used for this synchronization. Special runs in the beam-ON period are foreseen to study the effect of the beam flash on the gain.

In order to acquire the data from the monitoring box (4 Photodiodes) in the T-DAQ room we will use 1 calorimeter like ROC so that we will receive here in input: (1) one system Clock Fiber and (2) one Control Optical Fiber. In output, we will provide 1 data fiber for readout. During calibration runs, we will acquire also another "special" calorimeter like ROC to read-out the 8 monitoring Pin Diodes inside the DS.

References

[1] R.Bernstein et al., "Calorimeter requirements", Docdb # 864 (2014).
[2] B. Aubert et al., "The BABAR detector", Nucl. Inst. and Meth. **A479** p1 (2002).
[3] T. Radicioni, "Calibration and performance of the Electromagnetic calorimeter in Mu2e", diploma Thesis, Univeristà di Pisa 2016. Mu2e-doc-8389 (2016).
[4] M.Angelucci et al., " Longitudinal uniformity, time performances and irradiation test of pure CsI crystals", Nucl. Inst. and. Meth. **A824** p678 (2016), S. Baccaro et al., "Irradiation study of UV silicon photomultipliers for the Mu2e calorimeter", **JINST 12** (2017) C02022.
[5] M. Anfreville et al., "Laser Monitoring system for the CMS lead tungstate crystal calorimeter ",Nucl. Inst. and Meth. **A594** p292 (2008).
[6] N. Atanov et al.,"Measurement of time resolution of the Mu2e LYSO calorimeter prototype", Nucl. Inst. and Meth. **A812** p104 (2016).
[7] N. Atanov et al., "The Mu2e Calorimeter Final Technical Design Report", Docdb # 8429 (2016).
[8] N. Atanov et al., " Design and status of the Mu2e crystal calorimeter", proceeding for Scint-2017 conference, submitted to IEEE (2017).
[9] R. Kwarciany et al., " TDAQ Timing Distribution Specifications", Docdb # 7048 (2016).